International Journal of Bioprinting

RESEARCH ARTICLE

Multifunctional high-simulation 3D-printed hydrogel model manufacturing engineering for surgical training

Xiaodong Xu[1,2†], Shijie Yu[1,2†], Liang Ma[1,2], Jinlei Mao[2,3], Hao Chen[2,3], Zhihao Zhu[2,3], Li Wang[4], Hui Lin[5], Jing Zhang[1*], Zhifei Wang[2*]

[1]College of Materials Science and Engineering, Zhejiang University of Technology, Hangzhou, Zhejiang 310014, China

[2]Department of Hepatobiliary & Pancreatic Surgery and Minimally Invasive Surgery, Zhejiang Provincial People's Hospital, Hangzhou, Zhejiang 310014, China

[3]The Second Clinical Medical College, Zhejiang Chinese Medical University, Hangzhou, Zhejiang 310053, China

[4]Department of Ultrasound Medicine, Zhejiang Provincial People's Hospital, Hangzhou, Zhejiang 310014, China

[5]College of Biomedical Engineering and Instrument Science, Zhejiang University, Hangzhou, Zhejiang 310058, China

[†]These authors contributed equally to this work.

***Corresponding authors:**
Jing Zhang
(zhangjing@zjut.edu.cn)

Zhifei Wang
(wangzhifei1973@zju.edu.cn)

Citation: Xu X, Yu S, Ma L, *et al*., 2023, Multifunctional high-simulation 3D-printed hydrogel model manufacturing engineering for surgical training. *Int J Bioprint,* 9(5): 766.
https://doi.org/10.18063/ijb.766

Received: February 23, 2023
Accepted: April 18, 2023
Published Online: June 1, 2023

Abstract

Advanced bionic organ models with vivid biological structures and wetness and softness are essential for medical-surgical training. Still, there are many challenges in the preparation process, such as matching mechanical properties, good feedback on surgical instruments, reproducibility of specific surgical scenarios, and distinguishability between structural levels. In this paper, we achieved tissue-mimicking dual-network (DN) hydrogels with customizable stiffness by adjusting the composition of the hydrogel matrix and the immersion time of the ionic solution to match different biological soft tissues precisely. Combined with advanced three-dimensional (3D) printing fabrication techniques, various performance-tunable bionic hydrogel organ models with structural complexity and fidelity, including kidney, liver, pancreas, and vascular tissues, were perfectly fabricated. The simulation and applicability of the model were also simulated for the forced change of the suture needle in the puncture and suture of a single tissue and between different tissues, the cutting of substantive organs by ultrasonic scalpel, the coagulation and hemostasis of blood vessels, the visualization of the internal structure under ultrasound, and the microwave ablation of liver tumors. By constructing advanced biomimetic organ models based on hydrogel with specific and tunable properties, the development of surgical training, medical device testing, and medical education reform will be significantly promoted.

Keywords: Bionic organ models; 3D printing fabrication; Surgical training; Dual-network hydrogels; Tunable properties

1. Introduction

In clinical surgery, laparoscopic and robotic surgeries are developing rapidly. Still, due to the high complexity of the procedures, training surgeons in surgical operations is essential to ensure safe and effective completion of these surgical treatment procedures. Training can help surgeons safely and efficiently navigate the learning curve of many surgical procedures that are operationally difficult and costly in terms of trial and error, further enhancing surgeon confidence, improving medical level, and reducing surgical risk[1,2]. With advances in surgical care systems, the establishment of quality assurance goals, expensive operating room time and increased surgical complexity, and a greater emphasis on patient safety, the traditional single model of relying on surgical skills acquired from the operating room experience has led to a significant decrease in surgical training for young surgeons. Particularly in special times like the novel coronavirus epidemic, many hospitals have significantly reduced emergency and elective surgical volumes, and new challenges have been posed for training time and caseload training standards[3]. Indeed, it is unethical and unacceptable for students at any level of training to perform new techniques directly on patients[4]. Regulatory authorities such as the American Council for Accreditation of Medical Education (ACGME) require that surgeons be provided with surgical simulation programs to complete surgical training in the laboratory to meet the requirements. However, the current status of surgical operative training for surgeons in China could be better. Due to differences in medical conditions, young surgeons have few opportunities to perform hands-on surgery. Jiang *et al*. concluded that the most significant challenge facing young Chinese surgeons and surgical trainees is the need for more opportunities for hands-on learning[5].

With the increasing demand for surgical training, digital simulators such as virtual reality (VR) have been gradually applied in some large medical centers[6,7]. However, digital surgical simulation training is not only expensive, but surgical training with these models is only at the primary level. Advanced surgical simulation training consists of two types: biological models (*in vivo* and *in vitro*) and simulated physical organ models. The disadvantages of biological models are the individual differences, high cost and ethical implications, the risk of infection and contamination, and the inability to simulate specific scenarios in some surgeries, which are the key to surgical risks that can arise due to unfamiliarity[8]. Compared with the direct use of live organs or animal experiments, or even human clinical experiments, simulated physical organ models have the advantages of being low cost, ethical, and easy to operate and execute[9]. Through reasonable structural design and material selection of physical organ models, it is also possible to provide an environment similar to physiological characteristics and suitable for surgical operations, which is important for conducting medical skills training and robotic surgery simulation training for doctors and nurses.

In recent years, simulated physical organ models have been gradually introduced into surgical training[10,11]. In the era of robotic surgery, it is impractical to purchase the da Vinci surgical robot, which is worth of multimillion dollar, specifically for training in wet models (animal or fresh human cadavers or animal organs), and it is less feasible to apply surgical robots in hospital operating rooms for the aforementioned wet model training. The risk of losing the sense of touch with a completely new operating platform owing to insufficient specialized training has become an international concern. The use of simulated physical organ models instead of living organisms for surgical training has become a frontier hot research direction in the field of medical simulation research, with significant application advantages and prospects. However, most of the previous studies have used silicone materials and single-function hydrogel material models[12-15], which cannot provide a good realistic sensation of suture and surgical electric instrument cutting as well as wet and soft biological tissues due to the variability of their physicochemical structural properties. In addition, the surgical responses generated by electrosurgical instruments such as ultrasonic scalpel and ligasure and even electrocoagulation effect, which are routinely used in the current surgical simulation process, cannot be simulated, such as electrocoagulation operation to make the material to be realistically coked and thus coagulated to stop bleeding, ultrasonic scalpel to cut substantial organ realism, and coagulation to close blood vessels. Usually, surgical procedures are dissected along layers of tissue, which requires materials that need to reflect the nuances between layers in the simulation model, which is difficult to achieve with current models[16]. These are precisely the difficulties faced by the current bionic gradient structured soft models for surgical training and are the key to the design of surgical training models.

As a wet and slippery soft material, hydrogel is a class of hydrophilic polymeric materials with a three-dimensional (3D) network structure, whose 3D polymer network is filled with a large amount of bound water, interfacial water, and free water media[17]. Hydrogels have physiological characteristics similar to biological tissues and organs, which are also widely used in biomedical research[18]. In addition, the processing and preparation techniques and design solutions of hydrogels have been gradually improved due to the rapid development of 3D printing technology, a fast-prototyping method that generates 3D objects directly from computer-aided design (CAD)

data in a computer. It is a comprehensive technology that combines CAD, computer numerical control (CNC), mechanical technology, and materials science with a fundamental approach to the layered overlay. The CAD model is divided according to a specific layer thickness and then printed by a 3D printer with different capabilities using particular materials. The nozzles or optics are computer driven to form the structure on the substrate one layer at a time and build the complete object layer by layer. With the advancement of 3D printing platforms, various *in vitro* 3D tissue and organ structures with complex anatomical features, adjustable dimensions, and high spatial resolution can be easily and quickly constructed through a layer-by-layer process. The team summarized the current mainstream 3D printing technologies and the materials applied to different technologies in a specific classification. The latest technologies in organ model preparation and the contribution of 3D-printed organ models to various surgical procedures were reviewed[19]. In addition, Ng *et al*. made a detailed summary and evaluation of extrusion, stereolithography, and inkjet printing based on bio-3D printing. They provided a detailed classification overview of relevant hydrogel printing materials and application scenarios[20].

Hydrogels also offer highly tunable mechanical properties (stiffness, elasticity, and durability), similar to the strength of natural soft tissues. Such tunable properties can be used to construct 3D tissue and organ models with tissue-mimicking and mechanical characteristics. For example, Jiang *et al*. achieved hydrogel-based organ human models with interconnected cavities and gradient structures by developing metal ion-induced interfacial supramolecular assembly of hydrogel layers on 3D-printed fugitive hydrogel templates[21]. Additionally, Wang *et al*. used gelatin methacrylate (GelMA)/hyaluronic acid methacrylate (HAMA) ink and digital light processing (DLP)-based 3D printing to fabricate a variety of volumetric soft tissues with tissue-matched mechanical properties and structurally complex structures[22]. Yang *et al*. prepared heterogeneous hydrogels with complex shapes and fatigue resistance consisting of rigid skeletons and soft matrices by stereolithography bio gel tissue[23]. Nevertheless, due to their weak and poor mechanical properties, most dual-network (DN) hydrogel materials can barely meet the general modulus requirements of different tissue and organ models[24]. Based on this, we prepared a DN hydrogel with elastic properties using polyvinyl alcohol and acrylamide as the main monomer components according to the general characteristics of surgery and the physicochemical properties and structural morphology of human organs. We obtained a wet-slip hydrogel elastic material with mechanical and related physicochemical properties that can be selected in a wide range by adjusting the concentration of components and ionic solution immersion strategy. By combining 3D-printing technology, we designed and prepared physical models with various mechanical properties matching human organ tissues and used them for surgical training tests in different scenarios. It provides new strategies and solutions for future surgical training and medical device testing and has broad application prospects.

2. Materials and methods

2.1. Materials

The materials used in the study include polyvinyl alcohol (PVA, 98–99% alcoholysis, Aladdin), acrylamide (AM, 99%, Aladdin), N-N'-methylene-bis-acrylamide (MBAA, 99%, Aladdin), ammonium persulfate (APS, >98%, Aladdin), tetramethylethylenediamine (TEMED, ≥ 99.5%, Aladdin), sodium chloride (NaCl, 99.8%, Aladdin), aqueous dyes, and deionized water. All materials were bought and used directly without further purification.

2.2. Preparation of hydrogel models

The preparation of the pre-polymerization solution of the model was mainly done in two parts. Firstly, PVA was dissolved at 90°C for about 1 h until the solid powder was dissolved entirely, cooled to room temperature, and then bottled to obtain solution A. Then, 2 M of AM was dissolved in deionized water at room temperature, and 0.03–0.3 mol% of MBAA and 2 mg/mL of APS were added to obtain solution B. Solution A and solution B were mixed at a volume ratio of 1:1 and stirred evenly. Finally, 2 μL/mL TEMED solution was added dropwise to obtain the pre-polymerization solution. The pre-polymerization solution was injected into the 3D-printed organ molds prepared in advance through the pouring port until they were full. Then the whole molds filled with the solution were put into a freezer at -20°C for a cryogenic freezing reaction and removed from the freezer. Depending on the desired conditions of the model, 1–2 cycles of freezing were performed, and the prepared hydrogel model was finally detached from the mold after room temperature was restored. For the pipeline models of the category of blood vessels with similar fine apertures, the blood vessel models were obtained by printing the sacrificial material as the inner core, coating the surface with the pre-polymerization solution, and waiting for the end of the reaction to remove the inner core. The various organ models obtained were treated by immersion in a saturated NaCl solution of choice according to the requirements to get the final training model that met the performance requirements.

2.3. Mechanical property tests

The hydrogel samples were tested by Instron Model 5576 (USA) universal material testing machine with a 10 kN load cell. Dumbbell samples (25 × 4 × 2 mm) for tensile experiments were tested at the tensile rate of 100 mm/min, and cylindrical samples (d = 8 mm, h = 6 mm) for compression experiments were tested at the compression rate of 5 mm/min. The Young's modulus of the hydrogel was calculated from the slope of the stress–strain curve, ranging from 10% to 20% of the strain.

2.4. Electrical conductivity tests

The conductivity of the hydrogels was measured by a digital four-probe tester (RTS-9, 4 PROBES TECH) with a current of 10 μA and a linear probe tip (1.0 mm spacing). Each sample was tested 10 times and averaged. All hydrogels were washed with deionized water, and residual water was removed from the hydrogels using filter paper.

2.5. Thermal conductivity tests

The thermal conductivity of the prepared hydrogel samples was measured at room temperature by the transient planar heat source method using a Hot Disk thermal constant analyzer (TPS 2500 S, Hot Disk, Sweden). All measurements were performed three times.

2.6. Rheology testing

The viscoelasticity of all hydrogels was evaluated by an advanced expanded rheometer (MCR302, Anton Paar) with a parallel plate with a diameter of 25 mm. Hydrogel sheet samples of 25 mm diameter and 1.2 to 1.8 mm thickness were placed under the top plate.

Dynamic sweep tests (from 0.1 to 100 rad/s) were first performed at constant strain (ε = 0.1%) to determine the viscoelasticity (tan δ, G"/G'), where G' and G" are the storage modulus and loss modulus, respectively. Next, the variation of the friction coefficient with time under constant normal force (F = 5 N, ω = 0.5 rad/s) was tested for 15 min with a friction coefficient μ = 4T/3RF (where T is the torque and R = 12.5 mm). It is worth mentioning that during the friction test, the tissue-like soft hydrogel was dripped with an appropriate amount of deionized water to prevent the sample from becoming dehydrated and dry.

2.7. Surgical needle suturability study

The test was performed by an Instron Model 5576 (USA) universal material testing machine connected to a 500 N load cell. A 0.6 mm diameter straight needle was manually held by a clamp, and the sample was punctured at a speed of 60 mm/min, during which force and displacement data were recorded. Two samples with different stiffnesses were also pierced continuously at the same feed rate, and the force and displacement data were recorded from the beginning of the first sample to the end of the second sample.

2.8. Ultrasonic scalpel cutting tests

Hydrogel models of different substantial organs, such as liver and kidney, were prepared separately. The surgical cutting process of real tissues was simulated using ultrasonic scalpel instruments to evaluate the smoothness and realism of the models in the cutting process. The vibration frequency of the blade head of the ultrasonic scalpel was set to 55 kHz.

2.9. *In vitro* vascular clotting and hemostasis study

Hydrogel blood vessel models with different diameters of 1, 2, and 3 mm were designed, respectively. They were placed in molds in advance, and the prepared hydrogel liquid was poured into the molds for curing to obtain the samples containing vascular channels inside. To simulate the surgical scenario more realistically, the low power grade of the ultrasonic scalpel was chosen to coagulate the vessels separately to avoid possible thermal damage to the tissue. In addition, the blood flow process was simulated by connecting a pressure-adjustable circulation pump system to the outside world to simulate the coagulation and hemostasis of the ultrasonic scalpel in an accidental bleeding scenario during surgery.

2.10. Microwave ablation study of tumors

The sample with the tumor simulant was prepared first, and the power parameters could be set to vary from 50 to 80 W, and the time could be set from 2 to 5 min depending on the size of the tumor and the treatment situation. In this experiment, we prepared an ellipsoidal tumor sphere with a long axis of about 2.5 cm and a short axis of about 1.5 cm, which was implanted in a sample simulating the liver parenchyma for anatomical photography. The ablation needle of a microwave ablation therapy instrument (KY-2000A, Kangyou Medical Devices Co. Ltd., China) with a power of 65 W and a time of 3 min was inserted into the tumor mimic. Then the instrument was started to observe the changes in the tumor during ablation. This process can be completed under the guidance of ultrasonic devices.

2.11. Ultrasonic image tests

The internal structure of the model with tubes was observed by the Welld full digital ultrasound (Shenzhen Welld Medical Electronics Co. Ltd., China) after the model was passed into the fluid and discharged from the air. The ultrasound frequency could be selected in a low- or high-frequency mode according to training needs. A little ultrasonic coupling agent was applied to the surface of the observed object so that the ultrasonic probe and the observed object could be closely combined, thus reflecting

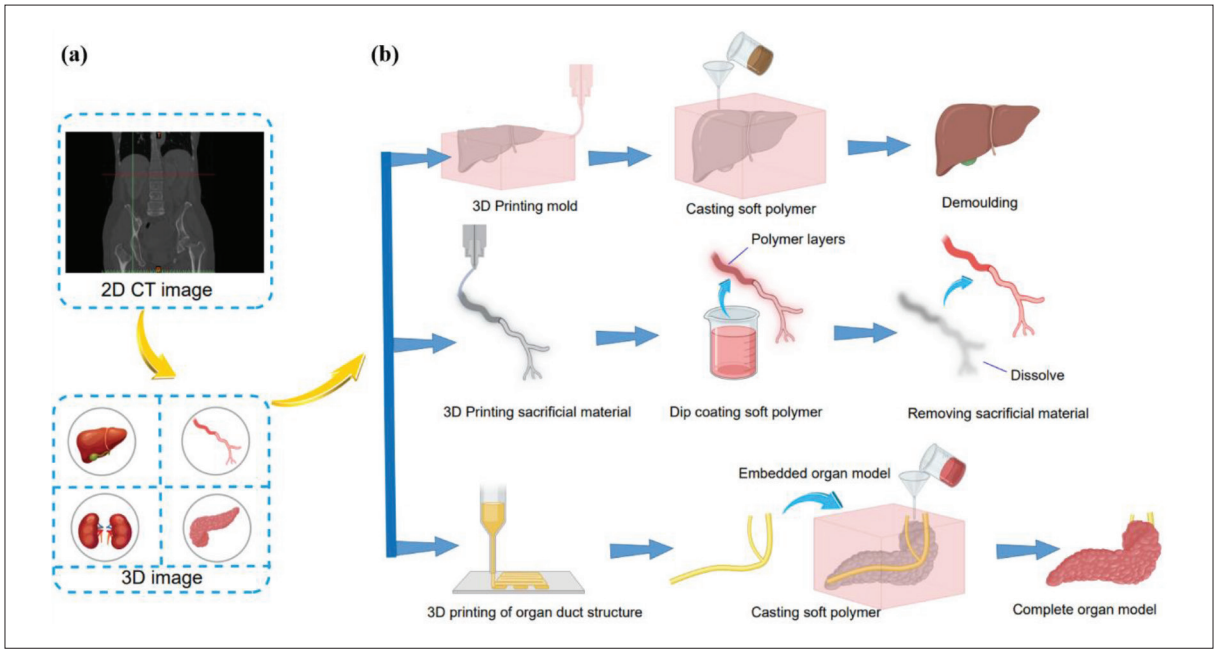

Figure 1. Schematic illustration of (a) computer extraction of organ files and (b) models preparation process.

the internal situation of the model more clearly and accurately.

2.12. Statistical analysis

Software of Microsoft Excel 2016 was used to implement the statistical analysis. All the data were expressed as the mean or means ± standard deviations (SD). The statistical analysis was performed with a Student's *t*-test. If the *P* value is lower than 0.05, the difference is considered significant. The number of samples is three in each test.

3. Results and discussion

3.1. Preparation of hydrogel training models

As shown in Figure 1a, anonymous medical digital image files were obtained using the MIMICS 23.0 system from 3D computed tomography scans of the human abdomen, and anatomical models of the liver, kidney, and pancreas were extracted and reconstructed. The extracted STL files were imported into Magic 24, where the models were repaired to obtain a finer structure. Then, the OBJ files were exported from Magic 24 and imported into Z Bush for further modifications. Finally, mold naming was done through NX 1899, and the positive and negative molds were designed according to the shape of the organ. The STL file of the designed mold was imported into Magic 24 for further design of the support structure and positioning. Next, the FDM 3D printer was used to print the molds based on the slice data, and after printing, the molds were surface treated, and the support structures were removed. Ultimately, according to the requirements of different organ structures and training functions, we can choose the direct one-step casting or dip coating hydrogel materials to construct the organ models, or we can select the two-step method of first printing and then casting to prepare relatively more complex organ models. Regarding this method, the internal structure of the organ model is first printed using water-soluble PVA filament, then embedded in a mold with a slot and cured by injecting hydrogel pre-polymer to get the final model. This solution is mainly used for ultrasonic inspection of the training model because the dissolved PVA filament and the hydrogel matrix part will have interface differences. The internal structure distinction can be seen under ultrasonic. The model preparation scheme is shown in Figure 1b.

3.2. Physicochemical and mechanical properties' characterization of hydrogel training models

In this paper, we propose a DN elastomeric hydrogel with tissue softness to achieve target tissue-matched mechanical properties whose mechanical properties can be modulated in a wide range by adjusting the hydrogel composition concentration and immersion time in ionic solutions.

Typically, pristine polyvinyl alcohol/polyacrylamide (PVA/PAM) hydrogels are soft and have low strength. The gel strength of PVA/PAM hydrogels was increased by immersion in a saturated NaCl aqueous solution. The effects of immersion time and PVA component concentration on the mechanical properties of PVA/PAM hydrogels were studied. The tested hydrogel samples were named as X% PVA/PAM-Y h. X indicates the mass

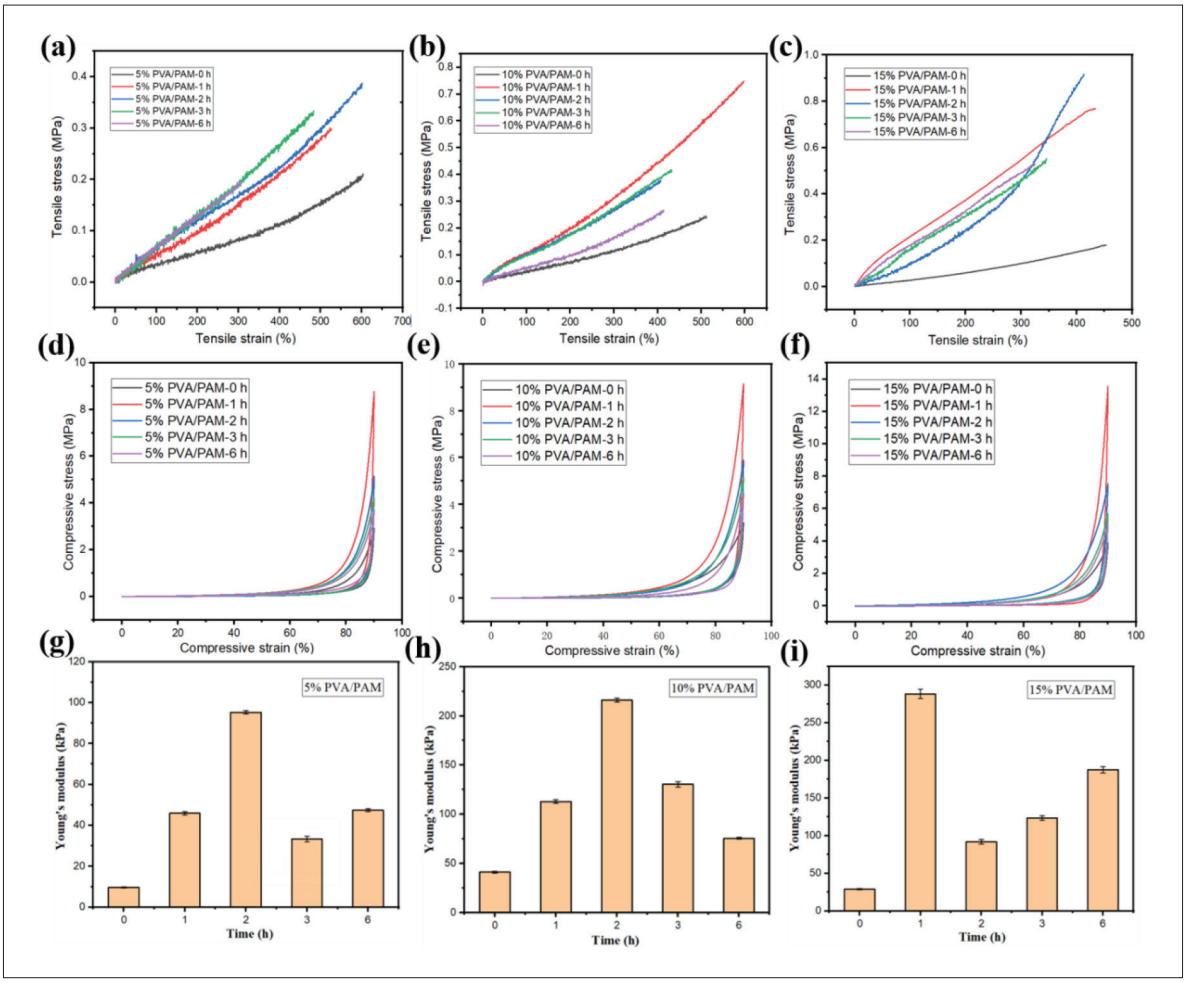

Figure 2. Mechanical properties of tissue simulation hydrogels. (a–c) Tensile stress–strain curves of 5% PVA/PAM hydrogel, 10% PVA/PAM hydrogel, and 15% PVA/PAM hydrogel immersed in saturated NaCl solution for different time. (d–f) Compressive stress–strain curves of 5% PVA/PAM hydrogel, 10% PVA/PAM hydrogel, and 15% PVA/PAM hydrogel immersed in saturated NaCl solution for different time. (g–i) Young's modulus of 5% PVA/PAM hydrogel, 10% PVA/PAM hydrogel, and 15% PVA/PAM hydrogel immersed in saturated NaCl solution for different time.

fraction of PVA solution used to participate in the reaction, and Y indicates the time of immersion of the reacted DN hydrogel in saturated NaCl solution. The typical stress–strain curves of various PVA/PAM hydrogels are shown in Figure 2. It can be seen that the tensile (Figure 2a–c) and compressive (Figure 2c–f) strengths of PVA/PAM hydrogels can be significantly increased by the immersion strategy, and the concentration of PVA components has relatively little influence on the results. The results indicate that this immersing method is a simple and effective method for improving the mechanical properties of PVA/PAM hydrogels. The tensile strengths of the original PVA/PAM hydrogels of each concentration were about 0.2 MPa, and the compressive strengths were about 3 MPa, which were enhanced to different degrees after immersion. In particular, the tensile strength of PVA/PAM hydrogel increased to 0.9 MPa, and the compressive strength reached 14 MPa after 15% PVA/PAM was soaked in a saturated NaCl aqueous solution for 2 h. At the initial stage, the tensile and compressive strengths of PVA/PAM hydrogels increased with the extension of immersion time. When the immersion time exceeded 2 h, a decrease in the mechanical properties of PVA/PAM hydrogels could be observed. The densely crosslinked network structure of PVA/PAM hydrogels could be promoted by salt precipitation during the immersion process. The densely crosslinked network structure helps improve the mechanical properties of hydrogels. Chain entanglement may also occur during the immersion process. Chain entanglement also leads to an increase in tensile strength. However, when the soaking time exceeds 2 h, the high-density crosslinked network can severely affect the mechanical properties of PVA/PAM hydrogels. It was found that the high Fe^{3+} content in Fe^{3+} crosslinked polyacrylic acid/graphene oxide (PAA/GO)

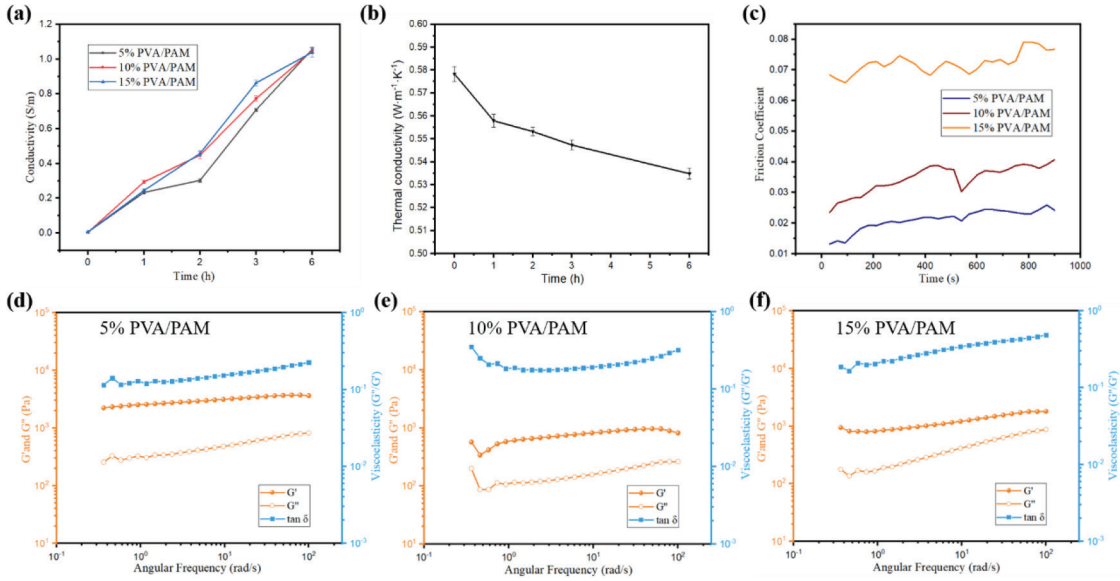

Figure 3. (a) Electrical conductivity of 5% PVA/PAM hydrogel, 10% PVA/PAM hydrogel, and 15% PVA/PAM hydrogel immersed in saturated NaCl solution for different time. (b) Thermal conductivity change curves of hydrogels immersed in saturated NaCl solution for different time. (c) Friction coefficient of 5% PVA/PAM hydrogel, 10% PVA/PAM hydrogel, and 15% PVA/PAM hydrogel immersed in saturated NaCl solution for different time. (d–f) Oscillation frequency sweep and viscoelasticity (tan δ, G″/G′) of hydrogels with different components, where G′ and G″ are the storage modulus and loss modulus, respectively.

hydrogels leads to a decrease in the tensile strength of the hydrogel at fracture[25]. As mentioned above, only reasonable immersion time can confer good mechanical properties to PVA/PAM hydrogels. It is well known that biological soft tissues have high flexibility and mild mechanical properties, while the stiffness varies widely from site to site[26]. As seen in Figure 2g–i, Young's modulus of our prepared elastic hydrogels is mechanically tunable over a wide range from a few kPa to hundreds of kPa, thus providing a promising candidate for the preparation of property-matched soft tissue mimics.

Upon immersion in an aqueous NaCl solution, NaCl will penetrate the crosslinked network of the PVA/PAM hydrogels. The combination of Na^+ and Cl^- in the hydrogels will impart electrical conductivity to the PVA/PAM hydrogels. The electrical conductivity of each group of PVA/PAM hydrogels was measured by a digital four-probe apparatus, and the results are shown in Figure 3a. The results suggest that the electrical conductivity of PVA/PAM hydrogels not immersed in saturated NaCl solution was lower than 0.01 S/m regardless of the increase in the concentration of PVA. The electrical conductivity showed an increasing form as the immersion time in saturated NaCl solution increased. The conductivity after 1 h of immersion exceeded 0.2 S/m, and the conductivity after 6 h exceeded 1 S/m, which can meet the conductivity requirements of most human tissues[27,28]. Therefore, we can choose the appropriate immersion strategy to obtain the required surgical training model with conductivity and matching mechanical properties by controlling the immersion time. In addition to the electrical properties, the thermal properties of the model are also important factors that cannot be ignored. In many surgical procedures, surgical electrical instruments often require energy transfer in many cases to achieve the final target effect. Figure 3b shows that with the increase of sample immersion time, the thermal conductivity decreased from 0.58 to 0.54 W/m/K. Despite the decrease, the entire value of thermal conductivity is close to that of human or animal tissues[29]. These characteristics benefit all energy surgical instruments to have a better realistic experience when trained on the model.

Rheological measurements were also performed to demonstrate the viscoelastic and wet-slip properties of tissue-like elastic hydrogels. Rheological frequency scans of the hydrogels confirmed that they exhibit dynamic viscoelastic behavior (Figure 3d–f). The energy storage modulus (G′) is consistently higher than the loss modulus (G″) over the entire frequency range, which strongly validates the solid elasticity characteristics of the hydrogels. Viscoelasticity of the tissue-mimic hydrogels was calculated as tan δ, namely, G″/G′ The results show that all tissue-simulated hydrogels with different viscoelasticity exhibit similar dynamic viscoelastic responses. The viscoelasticity of all these tissue-simulated hydrogels is in the range of 0.11–0.55, which is very similar to the viscoelasticity of

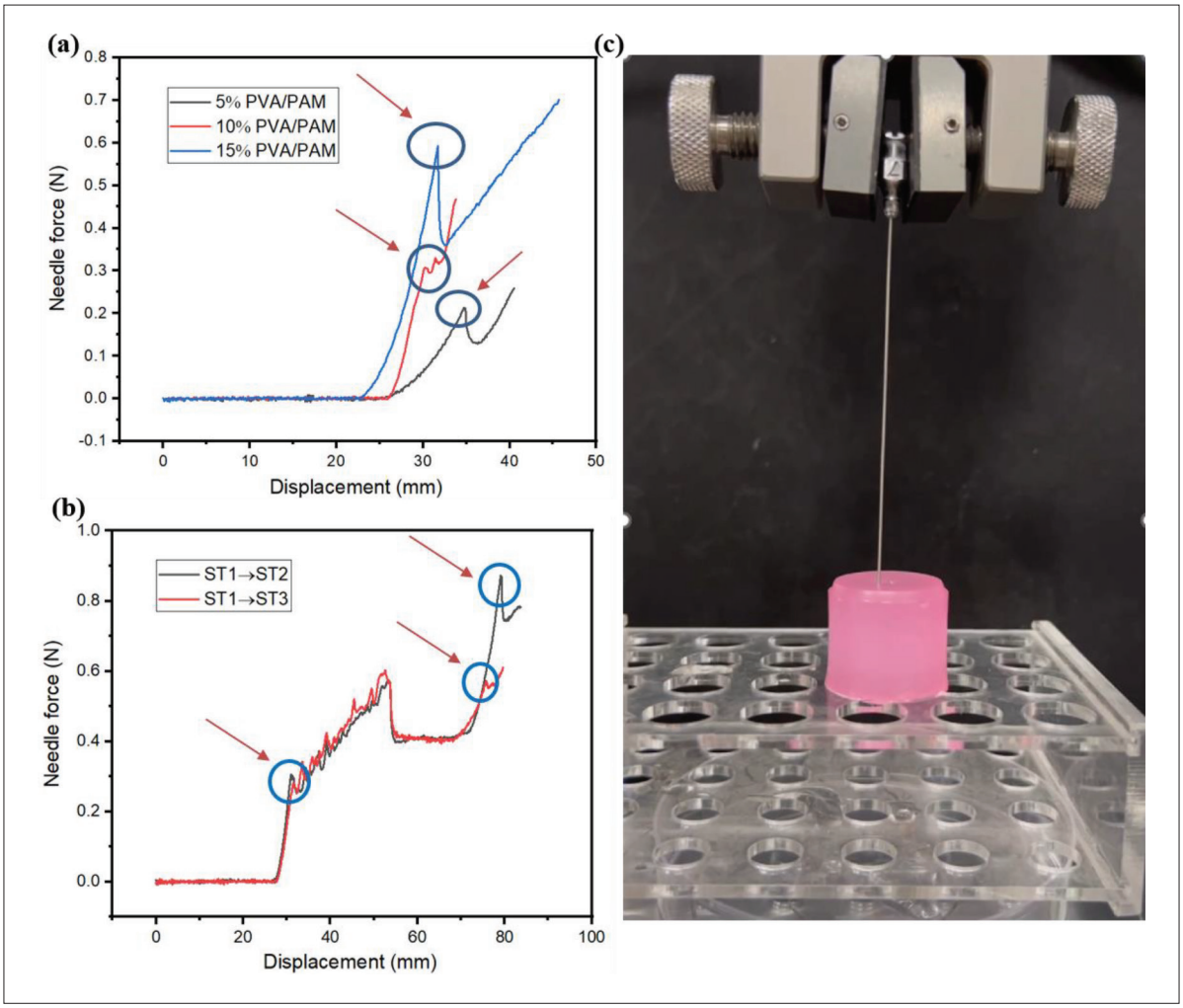

Figure 4. Force–displacement curves for simulated puncture sutures of single tissue samples (a) and suture needles of different tissue samples (b). Field test picture (c).

various living tissues. These results fully confirm that the softness of elastic hydrogels can be precisely adjusted to match multiple tissue and organ models with viscoelasticity similar to that of biological soft tissues. Furthermore, the tissue-like softness of the hydrogels significantly reduced friction due to their high water content and wettability (Figure 3c). In addition, the improved lubricity of these elastic hydrogels is due to the extrusion of water under load, exhibiting excellent slip properties[30].

3.3. Surgical instrument feedback characterization of hydrogel training model

Liver trauma is the most common and severe abdominal trauma, and timely suturing of the liver is especially important. Besides, various difficult surgical suturing training is also an ability consideration and professional quality improvement for surgeons. Figure 4a shows a typical force–displacement curve of a simulated surgical needle piercing into a tissue simulation sample at a speed of 60 mm/min. The presence of a distinct mutation point, which we call the puncture point, indicates that rupture has occurred, or in other words, that the needle tip has punctured the outer membrane of the model. During the needle insertion into the soft tissue, the relative motion between the needle and its surrounding tissues cannot be ignored[31]. The process is divided into two phases: the no-rupture phase (zero relative velocity) and the rupture phase (presence of relative motion). It can be seen that with the increase of PVA component concentration, the force required by the puncture point gradually increased from 0.2 to 0.6 N, which is in line with the range of force sizes required for the suture needle to puncture the suture target in human tissue during suturing[32]. Surgical suture often involves needle insertion between different tissues.

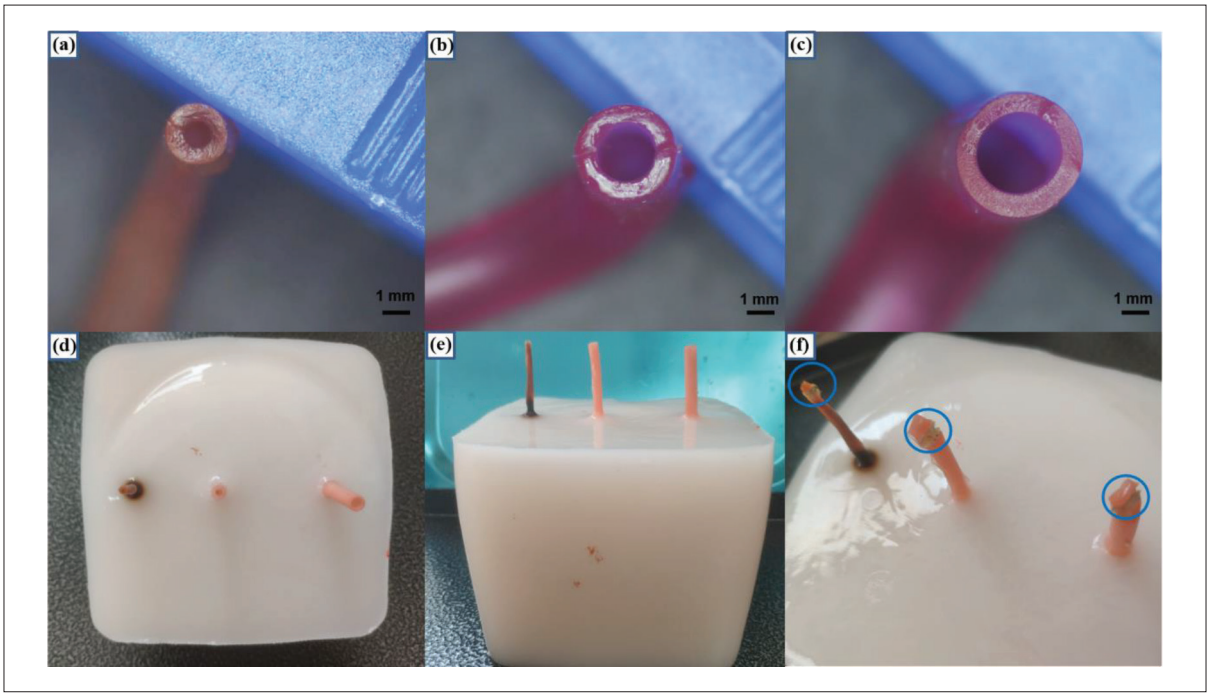

Figure 5. Microscopic illustration of (a) 1 mm, (b) 2 mm, and (c) 3 mm vascular models. (d, e) Top view and master view of the model with blood vessels. (f) Results of vascular coagulation.

Different tissues can vary in the force required to feed the needle due to differences in inter-tissue rigidity. As shown in Figure 4b, to better show the difference, three samples with different rigidity were selected to simulate different tissues, respectively. The sample group with medium rigidity was set as simulation tissue 1 (ST 1), the largest rigidity was set as simulation tissue 2 (ST 2), and the smallest was set as simulation tissue 3 (ST 3). The penetration process of different rigid tissues was simulated by controlling the needle feed from ST 1 group to ST 2 group and ST 3 group, respectively. It can be seen that the force magnitude of the first breakthrough point in Figure 4b is 0.3 N, and the second breakthrough points of the two experimental groups are about 0.5 and 0.15 N, respectively, which are consistent with the expected assumptions. The test scheme was recorded through the universal material testing machine to facilitate the accurate collection of force-related data. Figure 4c shows the field picture during the test, and the **Videoclip S1** (Supplementary File) is the specific process of the experiment. Overall, the softness and elasticity possessed by these hydrogel models mean that the contact resembles the mechanical characteristics of natural soft tissue. It is also conducive to better understanding and visualization of biological tissue and organ characteristics, accumulating clinical experience, and gaining a realistic sense of operation, which plays a crucial role in preoperative planning and medical education training.

Surgical energy devices that provide adequate hemostasis and allow accurate dissection of tissue are critical during surgical procedures, which are often accompanied by bleeding and other conditions. Unreliable tools and unskilled medical personnel can cause bleeding, damage to adjacent organs, and compromise visualization. Modern energy devices have evolved rapidly over the past few years to improve hemostasis control and tissue dissection accuracy significantly. This progress has minimized operative time, reduced collateral damage to surrounding tissues and blood loss, and significantly improved the outcomes of laparoscopic and open surgical procedures. Due to the modernization of instruments and the increased complexity of the surgery, training in surgical operations and proficiency in the use of surgical instruments are inevitable for surgeons. Intraoperative bleeding is a frequent occurrence during surgery and is an important detail that cannot be ignored and needs to be taken seriously. To simulate blood vessels' coagulation and hemostasis process *in vitro*, we designed and prepared vascular models with diameters of 1, 2, and 3 mm, as shown in Figure 5a–c. And these blood vessel models with different diameters were embedded in the hydrogel samples to obtain the models with internal access vessels, as shown in Figure 5d–e. Priority was given to the clotting test of blood vessels of different diameters under the low power of the ultrasonic scalpel to avoid overheating damage to the tissues. The results are shown in Figure 5f and **Videoclip S2** (Supplementary File). Furthermore, to more realistically

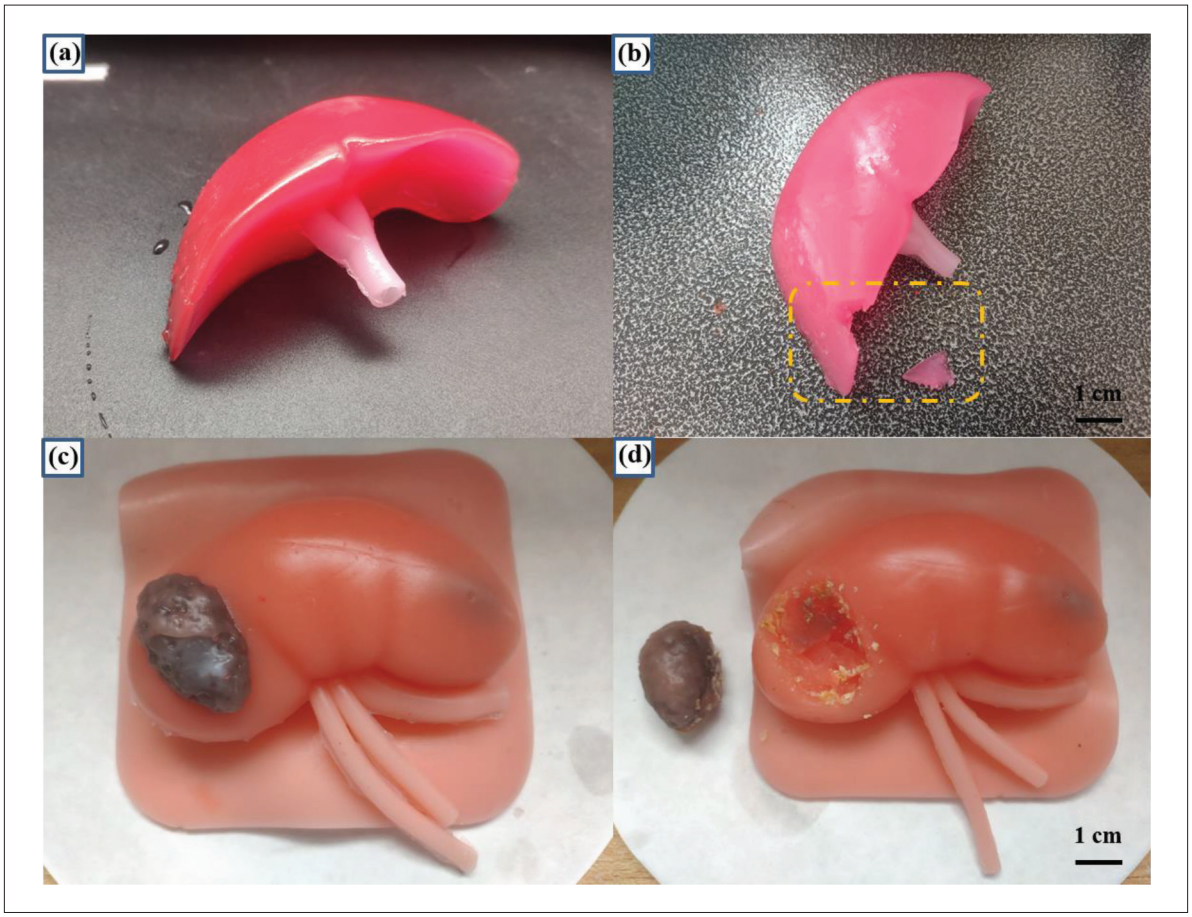

Figure 6. (a) Hydrogel liver model and (b) ultrasonic scalpel simulate liver parenchymal resection. (c) Hydrogel kidney tumorization model and (d) simulated tumor resection.

simulate the actual environment in surgery, the bleeding process of the blood vessel was simulated by connecting an external fluid circulation pump. The bleeding sample was coagulated and stopped using an ultrasonic scalpel. The process is shown in **Videoclip S3** (Supplementary File). In short, embedding tiny blood vessels in the model is expected to provide a scenario of unexpected occurrence for the training design of complex surgery and also serve as a standard for the technical evaluation of doctors in the surgical process.

For an advanced surgeon, suturing, knotting, and standard anatomical techniques are critical skills[33]. Surgical resection is currently the primary curative treatment for liver and kidney tumors. Surgeons are often tasked with ensuring adequate removal of tumors, minimizing intraoperative blood loss, and preserving good residual organ function. The most common complications of hepatic and nephrectomy include bleeding, intra-abdominal infection, and post-operative organ failure[34]. To ensure the safety of patients and reduce the mortality rate, surgeons have to put forward higher requirements on surgical skills. As shown in Figure 6, the formulation of 10% PVA/PAM-1 h was selected for the preparation of liver and kidney models, while the formulation of 15% PVA/PAM-1 h was chosen for the preparation of tumors. To evaluate the resectability of the completed model, an ultrasonic scalpel was used to simulate the resection of the marginal portion of the liver parenchyma. The actual resection flow was smooth and stable, as shown in Figure 6a–b and **Videoclip S4** (Supplementary File). In addition, the instrumentation response and the tumor removal effect of the tumor kidney model during the resection process were evaluated by the tumor resection of the kidney. As shown in Figure 6c–d, it can be known that the tumor was resected as a whole without excess residue, and the resection process was smooth and stable without excessive interference. The actual demonstration process of both resections is shown in **Videoclip S5** (Supplementary File).

In addition to surgical resection, microwave ablation of malignant liver tumors has many indications. The

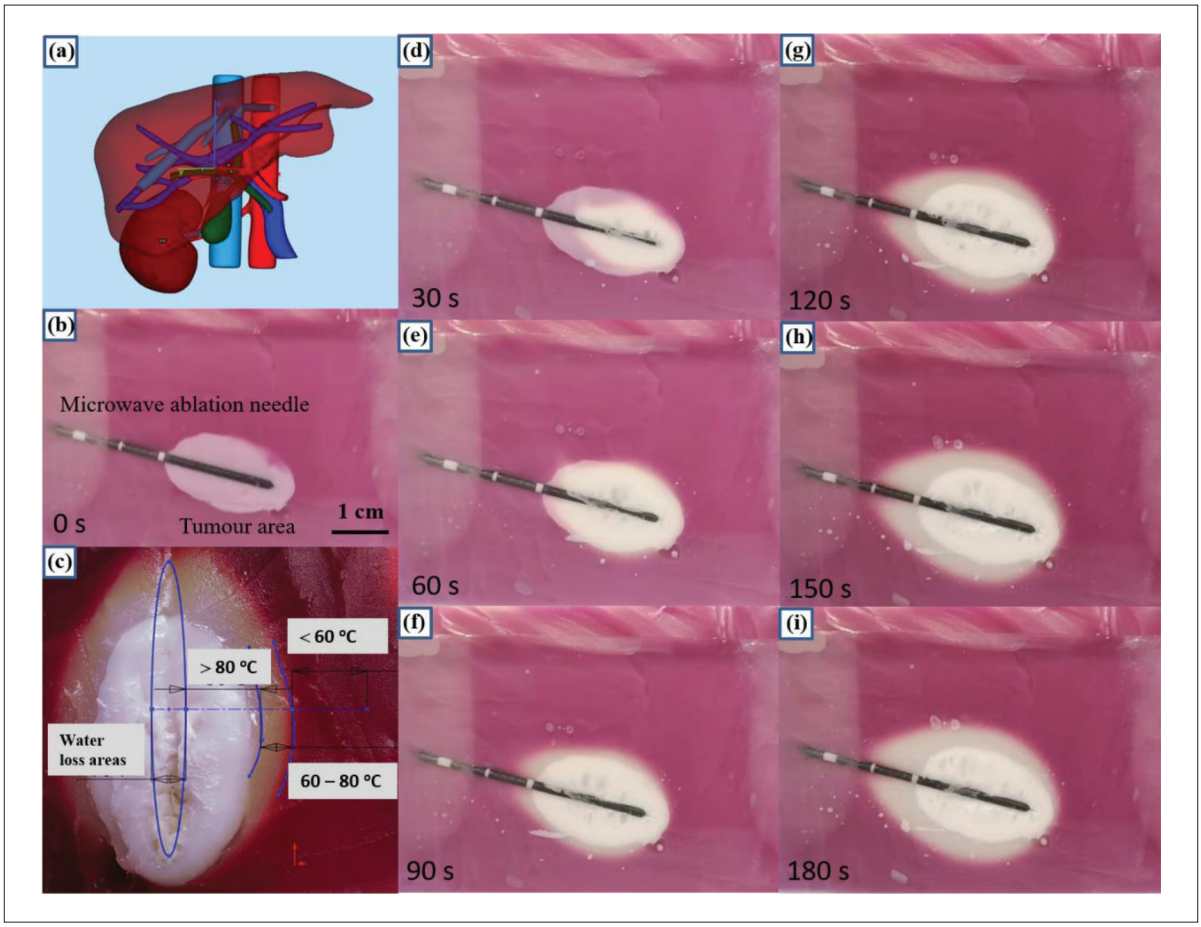

Figure 7. Simulation of microwave ablation of liver tumor model. (a) Conceptual diagram of the structure of the liver organ. (b, c) Cross-sectional view at the beginning and end of the treatment. (d–i) Cross-sectional view of different time periods of the ablation treatment process.

earliest application was mainly to treat tumors in patients unsuitable for surgical resection due to insufficient post-operative liver remnants, multinodular tumors, or patients who refused resection. Recently, microwave ablation has been increasingly applied as one of several treatments for small hepatocellular carcinoma[35]. The short-term and long-term results of microwave ablation for small hepatocellular carcinoma are comparable to surgery. It is a green treatment with both safety and exact efficacy. Figure 7a shows a conceptual drawing of a liver simulation containing complex internal structures. It is often necessary to avoid the complex systems inside the liver to reach the treatment area accurately under ultrasound guidance during the surgical treatment. To facilitate data recording, we designed a simple simulation sample of simulated liver parenchyma accompanied by tumor region. We dissected and inserted the needle tip part of microwave ablation into the tumor region, waiting for activation, see Figure 7b. Additionally, Figure 7c shows the temperature interval distribution after treatment. It can be seen that the middle needle insertion area has the highest temperature and belongs to the water loss area. The temperature gradually spreads outward through heat conduction. The white area part is more significant than 80°C, the yellow-white interval is 60–80°C, and the outermost part is less than 60°C. Combined with the thermal conductivity coefficient in Figure 3d, it shows that the material used in the model is consistent with the actual human body during the whole microwave ablation process, and the tumor can be ablated without a wide range of high temperatures. The tumor ablation process is shown in Figure 7d–i, and the video recording is shown in **Videoclip S6** (Supplementary File). In short, the design of this hydrogel model containing the tumor region allows for an *in vitro* realistic platform for the tumor ablation procedure, which will provide the trained surgeons with sufficient experience and skills for surgical treatment, thus improving the surgical quality and success rate of the process.

As mentioned above, ablation of liver tumors often requires ultrasound-assisted guidance to avoid intrahepatic

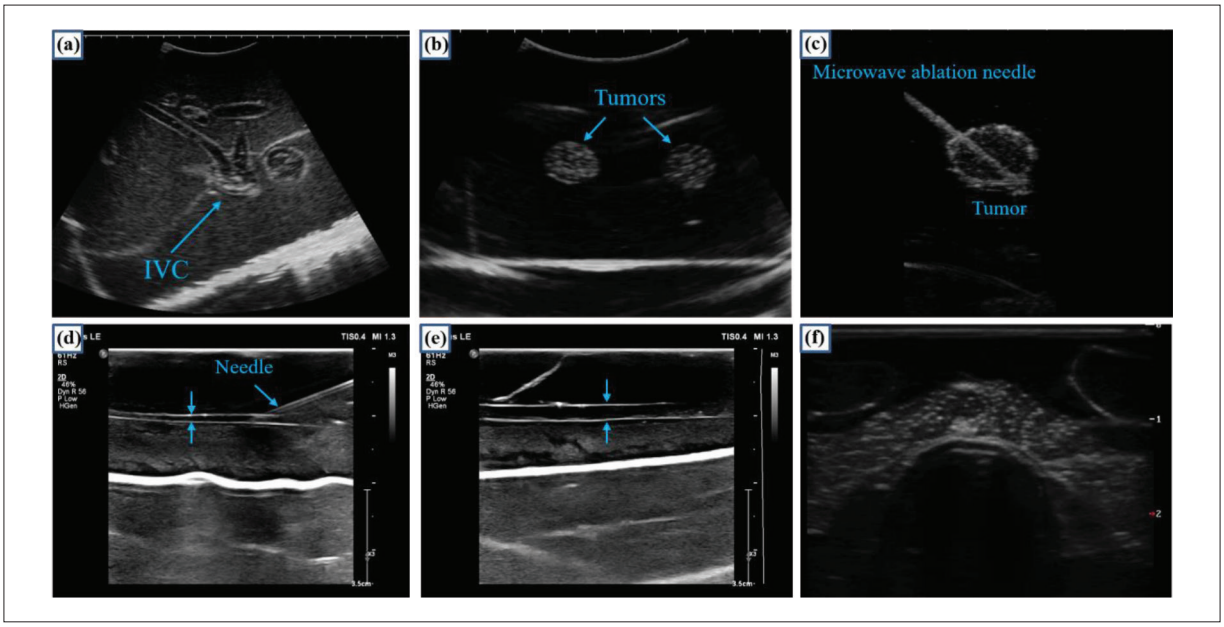

Figure 8. Ultrasonic images of hydrogel models of different organs. (a) Inferior vena cava structure of the hydrogel liver model. (b) Internal tumor of the hydrogel model. (c) The ablation needle is inserted into the designated tumor site under ultrasound guidance. (d, e) The small and large pancreatic ducts of the hydrogel pancreas model. (f) The structure of the thyroid gland in the hydrogel roaring neck model. IVC, inferior vena cava.

vessels, veins, and other structures and accurately reach the designated site for treatment. As shown in Figure 8a, the inferior vena cava (IVC) structure inside the liver model is presented under ultrasound at a frequency of 4–6 MHz, and the ductal access structure can be seen. Figure 8b–c shows ultrasound images of the tumor spheres designed to be detected inside the model and the accurate arrival of the ablation needle at the designated tumor area under ultrasound, respectively. In addition, we also simulated the ultrasound visualization of the internal structure of the pancreas in an actual situation by using an injection needle to continuously pass a flowing fluid in the pancreatic duct inside the pancreas, as shown in Figure 8d–e, where the entire interior is visible. To demonstrate the usability of the material in various models, in addition to the liver and pancreas models, we also tested the prepared thyroid model (**Figure S1** in Supplementary File). It was found that the test results still matched the actual human tissue and were consistent with the expected objectives, as shown in Figure 8f. In other words, the visualization of the internal structure of the hydrogel model can be achieved through the differentiated design of the matrix part and the internal construction of the model. This design solution will provide a novel and convenient platform for training and teaching many procedures.

4. Conclusion

In conclusion, we propose novel elastic hydrogels with tissue softness suitable for simulating tissue and organ models with biological structures and mechanical properties close to those of natural soft tissues. The mechanical properties of the elastic hydrogels were extensively regulated and precisely controlled by selecting the appropriate concentration of monomer composition and immersion time of the ionic solution. Various functionalized hydrogel organ models with structural and mechanical properties matching natural soft tissues, including liver, kidney, and blood vessels, were finely fabricated by combining various fabrication schemes of 3D printing. The prepared different organ models have physicochemical properties close to the actual human body, good feedback from surgical instruments, and realistic haptics and appearance. In addition, the designed models for hemostasis of blood vessels of different diameters, resection and ablation of the liver, and ultrasound-assisted visualization of internal structures can be used as practical clinical and surgical training platforms for *in vitro* simulation and training. In summary, the solution based on the combination of hydrogel tissue simulants with mechanically adjustable softness and advanced 3D printing manufacturing technology is considered to have a wide range of applications as a deployable platform for *in vitro* demand testing of new medical devices, preoperative rehearsal, and surgical training.

Acknowledgments

None.

Funding

This work was supported by the National Natural Science Foundation of China (21404091) and the Major Projects of the Ministry of Science and Technology (2018YFB1107104).

Conflict of interest

The authors declare no conflicts of interest.

Author contributions

Conceptualization: Xiaodong Xu, Jing Zhang, Zhifei Wang
Formal analysis: Xiaodong Xu, Shijie Yu
Investigation: Xiaodong Xu, Liang Ma, Hui Lin
Methodology: Xiaodong Xu, Hao Chen, Zhihao Zhu
Supervision: Jing Zhang, Zhifei Wang
Validation: Xiaodong Xu, Jinlei Mao, Li Wang
Writing – original draft: Xiaodong Xu, Shijie Yu
Writing – reviewing & Editing: Zhifei Wang, Jing Zhang

Ethics approval and consent to participate

Not applicable.

Consent for publication

Not applicable.

Availability of data

The data that support the findings of this work are available from the corresponding author, upon reasonable request.

References

1. Valdivieso RF, Zorn KC, 2014, Urological laparoscopic training—practice makes perfect. *Nat Rev Urol*, 11(3): 138–139.

   https://doi.org/10.1038/nrurol.2014.6

2. Panda N, Morse CR, 2020, Commentary: Practice makes perfect in cervical esophagogastric anastomosis. *J Thorac Cardiovasc Surg*, 160(6): 1611–1612.

   https://doi.org/10.1016/j.jtcvs.2020.04.018

3. Goldhamer MEJ, Pusic MV, Co JPT, *et al.*, 2020, Can covid catalyze an educational transformation? Competency-based advancement in a crisis. *N Engl J Med*, 383(11): 1003–1005.

   https://doi.org/10.1056/NEJMp2018570

4. Reznick RK, MacRae H, 2006, Medical education - teaching surgical skills - changes in the wind. *N Engl J Med*, 355(25): 2664–2669.

   https://doi.org/10.1056/NEJMra054785

5. The Lancet, 2016, The best science for achieving healthy china 2030. *Lancet*, 388(10054): 1851.

   https://doi.org/10.1016/S0140-6736(16)31842-6

6. Rudarakanchana N, Van Herzeele I, Desender L, *et al.*, 2015, Virtual reality simulation for the optimization of endovascular procedures: Current perspectives. *Vasc Health Risk Manag*, 11: 195–202.

   https://doi.org/10.2147/VHRM.S46194

7. Meola A, Cutolo F, Carbone M, *et al.*, 2017, Augmented reality in neurosurgery: A systematic review. *Neurosurg Rev*, 40(4): 537–548.

   https://doi.org/10.1007/s10143-016-0732-9

8. Chevallier C, Willaert W, Kawa E, *et al.*, 2014, Postmortem circulation: a new model for testing endovascular devices and training clinicians in their use. *Clin Anat*, 27(4): 556–562.

   https://doi.org/10.1002/ca.22357

9. Sandmann J, Mueschenich FS, Riabikin A, *et al.*, 2019, Can silicone models replace animal models in hands-on training for endovascular stroke therapy? *Interv Neuroradiol*, 25(4): 397–402.

   https://doi.org/10.1177/1591019919833843

10. Nagassa RG, McMenamin PG, Adams JW, *et al.*, 2019, Advanced 3D printed model of middle cerebral artery aneurysms for neurosurgery simulation. *3D Print Med*, 5(1): 11.

    https://doi.org/10.1186/s41205-019-0048-9

11. Giannopoulos AA, Mitsouras D, Yoo SJ, *et al.*, 2016, Applications of 3D printing in cardiovascular diseases. *Nat Rev Cardiol*, 13(12): 701–718.

    https://doi.org/10.1038/nrcardio.2016.170

12. Kaneko N, Mashiko T, Ohnishi T, *et al.*, 2016, Manufacture of patient-specific vascular replicas for endovascular simulation using fast, low-cost method. *Sci Rep*, 6(1): 39168.

    https://doi.org/10.1038/srep39168

13. Zhang Y, Xia J, Zhang J, *et al.*, 2022, Validity of a soft and flexible 3D-printed nissen fundoplication model in surgical training. *Int J Bioprint*, 8(2): 546.

    https://doi.org/10.18063/ijb.v8i2.546

14. de Jong TL, Pluymen LH, van Gerwen DJ, *et al.*, 2017, PVA matches human liver in needle-tissue interaction. *J Mech Behav Biomed Mater*, 69: 223–228.

    https://doi.org/10.1016/j.jmbbm.2017.01.014

15. Earle M, Portu GD, DeVos E, 2016, Agar ultrasound phantoms for low-cost training without refrigeration. *Afr J Emerg Med Rev Afr Med Urgence*, 6(1): 18–23.

    https://doi.org/10.1016/j.afjem.2015.09.003

16. Ratinam R, Quayle M, Crock J, *et al.*, 2019, Challenges in creating dissectible anatomical 3D prints for surgical teaching. *J Anat*, 234(4): 419–437.

    https://doi.org/10.1111/joa.12934

17. Liu X, Liu J, Lin S, *et al.*, 2020, Hydrogel machines. *Mater Today*, 36: 102–124.

https://doi.org/10.1016/j.mattod.2019.12.026

18. Ligon SC, Liska R, Stampfl J, *et al.*, 2017, Polymers for 3D printing and customized additive manufacturing. *Chem Rev*, 117(15): 10212–10290.

https://doi.org/10.1021/acs.chemrev.7b00074

19. Jin Z, Li Y, Yu K, *et al.*, 2021, 3D printing of physical organ models: recent developments and challenges. *Adv Sci*, 8(17): 2101394.

https://doi.org/10.1002/advs.202101394

20. Ng WL, Chua CK, Shen YF, 2019, Print me an organ! Why we are not there yet. *Prog Polym Sci*, 97: 101145.

https://doi.org/10.1016/j.progpolymsci.2019.101145

21. Jiang P, Ji Z, Liu D, *et al.*, 2022, Growing hydrogel organ mannequins with interconnected cavity structures. *Adv Funct Mater*, 32(13): 2108845.

https://doi.org/10.1002/adfm.202108845

22. Wang M, Li W, Hao J, *et al.*, 2022, Molecularly cleavable bioinks facilitate high-performance digital light processing-based bioprinting of functional volumetric soft tissues. *Nat Commun*, 13(1): 3317.

https://doi.org/10.1038/s41467-022-31002-2

23. Yang H, Ji M, Yang M, *et al.*, 2021, Fabricating hydrogels to mimic biological tissues of complex shapes and high fatigue resistance. *Matter*, 4(6): 1935–1946.

https://doi.org/10.1016/j.matt.2021.03.011

24. Zhao Z, Vizetto DC, Moay ZK, *et al.*, 2020, Composite hydrogels in three-dimensional in vitro models. *Front Bioeng Biotechnol,* 8: 611.

https://doi.org/10.3389/fbioe.2020.00611

25. Zhong M, Liu YT, Xie XM, 2015, Self-healable, super tough graphene oxide-poly(acrylic acid) nanocomposite hydrogels facilitated by dual cross-linking effects through dynamic ionic interactions. *J Mater Chem B*, 3(19): 4001–4008.

https://doi.org/10.1039/c5tb00075k

26. Guimarães CF, Gasperini L, Marques AP, *et al.*, 2020, The stiffness of living tissues and its implications for tissue engineering. *Nat Rev Mater,* 5(5): 351–370.

https://doi.org/10.1038/s41578-019-0169-1

27. Golberg A, Bruinsma BG, Uygun BE, *et al.*, 2015, Tissue heterogeneity in structure and conductivity contribute to cell survival during irreversible electroporation ablation by "electric field sinks". *Sci Rep,* 5(1): 8485.

https://doi.org/10.1038/srep08485

28. Joines W, Zhang Y, Li C, *et al.*, 1994, The measured electrical-properties of normal and malignant human tissues from 50 to 900 MHz. *Med Phys,* 21(4): 547–550.

https://doi.org/10.1118/1.597312

29. Yue K, Cheng L, Yang L, *et al.*, 2017, Thermal conductivity measurement of anisotropic biological tissue in vitro. *Int J Thermophys,* 38(6): 92.

https://doi.org/10.1007/s10765-017-2214-x

30. Liu D, Jiang P, Wang Y, *et al.*, 2023, Engineering tridimensional hydrogel tissue and organ phantoms with tunable springiness. *Adv Funct Mater,* 33(17): 2214885.

https://doi.org/10.1002/adfm.202214885

31. van Gerwen DJ, Dankelman J, van den Dobbelsteen JJ, 2012, Needle-tissue interaction forces - a survey of experimental data. *Med Eng Phys,* 34(6): 665–680.

https://doi.org/10.1016/j.medengphy.2012.04.007

32. Bao X, Li W, Lu M, *et al.*, 2016, Experiment study on puncture force between MIS suture needle and soft tissue. *Biosurface Biotribology,* 2(2): 49–58.

https://doi.org/10.1016/j.bsbt.2016.05.001

33. Grochola LF, Vonlanthen R, 2016, Surgical energy devices or devices for hemostasis. *Atlas Up Gastrointest Hepato-Pancreato-Biliary Surg,* 37–44.

https://doi.org/10.1007/978-3-662-46546-2_6

34. Chan YC, Li WF, Lin TL, *et al.*, 2013, Lin's clamp revisited: A safe model for training in liver resection. *Formos J Surg,* 46(2): 42–47.

https://doi.org/10.1016/j.fjs.2013.02.001

35. Liang P, Yu J, Lu MD, *et al.*, 2013, Practice guidelines for ultrasound-guided percutaneous microwave ablation for hepatic malignancy. *World J Gastroenterol,* 19(33): 5430–5438.

https://doi.org/10.3748/wjg.v19.i33.5430